A High-Power and Scalable 2-D Phased Array for Terahertz CMOS Integrated Systems

Yahya Tousi, *Member, IEEE*, and Ehsan Afshari, *Senior Member, IEEE*

***Abstract*—This work introduces a 2-D phased array architecture that is suitable for high power radiation at mm-Wave and Terahertz frequencies. We address the challenge of signal generation above the cut-off frequency of transistors by presenting a radiation method based on the collective performance of a large number of synchronized sources. As theory shows, both frequency locking/tuning and beam steering can be independently achieved by manipulating the local coupling between the nearest neighbors. This control method results in a dynamical network that is insensitive to array dimensions and is scalable to the point that can achieve a level of output power and spectral purity beyond the reach of conventional sources. To demonstrate the concept, we implement a 4×4 version of this phased array at 340 GHz using a 65 nm bulk CMOS process. The paper presents the design and implementation of the oscillators, couplings and the integrated antennas. The measured results at 338 GHz reveal a peak equivalent isotropically radiated power (EIRP) of +17.1 dBm and a phase noise of -93 dBc/Hz at the 1 MHz offset frequency. This chip presents the first fully integrated terahertz phased array on silicon. Furthermore, the output power is higher than any lens-less silicon-based source above 200 GHz and the phase noise is lower than all silicon radiating sources above 100 GHz.**

***Index Terms*—CMOS, coupled oscillators, distributed systems, phased array, radiator, scaling, terahertz.**

I. Introduction

INTEGRATED systems that operate in the sub-mm-wave frequencies will provide access to a region of the electromagnetic spectrum with unique physical properties including a plethora of molecular resonance bands, high absorption contrast toward moisture gradients, and high resolution imaging through most insulators that are otherwise optically opaque. Terahertz electronics has the potential to introduce a new wave of applications ranging from medical imaging of tissue surface, non-invasive industrial testing, material spectroscopy, to wide band secure communication.

In the last decade we have witnessed a large body of work on CMOS systems operating in the V-band and W-band, demonstrating applications in wide band communication [1]–[10], imaging, and sensing [11]–[16]. Today, this proliferation of mm-wave systems combined with the rich possibilities in sub-mm-wave frequencies has sparked interest in developing mm-wave systems that operate at frequencies closer to the terahertz spectrum [17]–[21]. Although compound semiconductors have clear advantages in terahertz electronics [22]–[25], the lower cost of CMOS transistors is reason enough to examine the potential of silicon based systems in sub-mm-wave frequencies.

Starting with terahertz detectors [26]–[29], recent work has also demonstrated the possibility of both probe-based and radiating sources close or above the cut-off frequency of CMOS devices that operate near and above the terahertz band. These works have attempted to tackle different aspects of this new field from exploiting devices close to their fundamental limits [30]–[32], employing novel radiation techniques [33]–[36], and developing new methods of signal generation and frequency tuning around 300 GHz [37]–[40].

Despite the interest in terahertz electronics, by approaching this frequency range particular hurdles start to appear that originate from fundamental limits in device scaling, as well as limitations in passive interconnections. Although nanoscale CMOS technology has brought us to the vicinity of this frequency band, we are at the final stages of the scaling roadmap and one can only expect modest improvements in the $f_{\max}$ of RF transistors as a result of further scaling [41]. On the other hand, device scaling has led to low operating voltages that by itself limits ultra-high frequency power generation both at the fundamental frequency and its harmonics. As a result, it would be hard to expect meaningful improvement in the operating frequency and performance of terahertz integrated systems originating from future scaling of CMOS technology. To further expand the territory of silicon transistors into the terahertz band, signal generation and processing needs to rely on more than the performance of individual devices. Structural scalability is a crucial aspect for integrated systems operating close to the physical limits of the device.

The foremost issue that any system operating at terahertz frequency needs to address is a flexible, integrated source that provides a decent level of radiated power. In general, the radiated power requirements vary with the application and depend on the distance of the source from the target, absorption and reflection properties of the material, and the sensitivity of the receiving detector. For instance, an active imager at 300 GHz with detection rate of 1 Kfps and a stand-off distance of 1 meter requires an isotropic radiated power of at least 100 mW, should it rely on the typical NEP levels achievable with CMOS detectors [26]–[28]. Such a power level is significantly higher than what the state-of-the-art has demonstrated using conventional circuits in CMOS for generating power above $f_{\max}$. Moreover, beside the generated power level, both the phase noise and the frequency tuning

Manuscript received July 25, 2014; revised November 05, 2014; accepted November 12, 2014. Date of publication December 18, 2014; date of current version January 26, 2015. This paper was approved by Associate Editor Jan Craninckx.

Y. Tousi is with the IBM T. J. Watson Research Center, Yorktown Heights, NY 10598 USA (e-mail: ymesgar@us.ibm.com).

E. Afshari is with Cornell University, Ithaca, NY 14853 USA (e-mail: ehsan@ece.cornell.edu).

Color versions of one or more of the figures in this paper are available online at http://ieeexplore.ieee.org.

Digital Object Identifier 10.1109/JSSC.2014.2375324

of the oscillators suffer as its operating frequency approaches $f_{\max}$. This is while for communication and spectroscopy applications as well as imaging arrays, phase and frequency tuning are essential both for modulation and beam steering.

To address this challenge, this work proposes a collective approach toward generation, radiation and control of terahertz signals. In this approach, while recognizing the effect of individual devices and circuits, we shift our attention to the collective performance of a large number of devices with scalable dynamics. For our purposes, a scalable structure has a functional characteristic that grows proportional to its dimensions without compromising its performance. In other words, a scalable structure needs to avoid building blocks that face performance degradation or introduce undesired complexity as the dimensions increase.

Based on this idea, in this work we present a scalable phased array which enables signal generation and radiation using multiple devices that operate synchronously and deliver a desired level of radiated power and phase noise at an operating frequency higher than $f_{\max}$. We demonstrate that the performance achieved by this structure exceeds the limitations of conventional sources or phased arrays due to an effective deployment of devices inside the system.

Starting with the next section, we provide the theoretical framework of this idea that is based on the concept of delay-coupled oscillators and then present a generalized form for Adler's model of electrical coupling between oscillators. Section III, presents the scalable two-dimensional phased array, the theory of core synchronization, and the meaning of scalability. This is followed by presenting the method for tuning the synchronized frequency of the array and steering the radiated beam. In Section IV we discuss circuit level implementation of this concept including integrated terahertz radiators, oscillators and interconnections. Finally, the last section, concludes the paper with chip prototype and measurement results, demonstrating the highest measured radiated power and the lowest phase noise of any integrated source above 200 GHz.

II. Locally Coupled Oscillators

This section begins with a different look into the dynamics of coupled electrical oscillators which proves to be a crucial piece in developing the idea of scalable phased arrays. First, we consider an electrical oscillator in steady state oscillation with a particular steady state orbit in the phase space. In the absence of any external influence the oscillator phase remains as a degree of freedom, randomly set at the onset of oscillation under the influence of thermal noise. However, as soon as an external signal is injected into the oscillator this uncertainly diminishes and a certain relation appears between the two phases of the oscillator and the injected signal. The equations that govern this type of coupling are known as Adler's equations who was the first to determine the relationship between the locking frequency of an oscillator and the resulting phase difference between the resonating core and the injected signal [42].

Fundamentally, what Adler's equation suggests is that in a system of coupled oscillators there is a mutual relationship between the locking frequency of two coupled oscillators and their relative phases. Injection locking applications are mainly concerned with setting the frequency of an oscillator to the predetermined frequency of the injecting signal. In such a configuration the phase between the two oscillators is set by the difference between the free-running frequency of the core oscillator and the locking frequency [38].

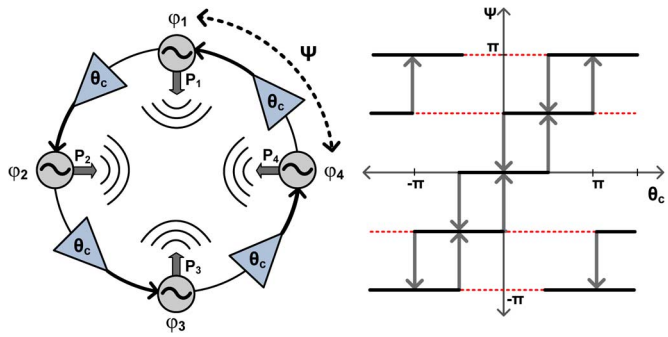

Fig. 1. Left: delay-coupled oscillators for frequency generation and radiation. Right: different possible phase shifts (ψ) between adjacent oscillators, and their stable region of operation as a function of the coupling phase shift, θ_c.

The idea of delay-coupled oscillator is based on the following observation: since there is a mutual relationship between the coupling phase and the locking frequency, it is possible to control the locking frequency of a system of coupled oscillators by fixing the coupling phase shift between adjacent cores. In other words it is possible to choose locking frequency as the degree of freedom that is subject to the phase shift of the injected signal. As demonstrated in Fig. 1, in a ring of N directionally coupled oscillators by manipulating the coupling phase shifts it is possible to both set the coupling mode of the system and tune the locking frequency. Even in the case the system initially settles to an undesired mode, by manipulating the coupling phase shifts it is possible to move the oscillators into the desired coupling mode.

There are two important advantages in using this oscillation system: 1) the phase shifters are buffered from the core oscillator and do not affect the quality factor of the resonator. As a result, this structure can be used to generate terahertz power from core transistors and at the same time tune the frequency without compromising the generated power. 2) The connection between oscillators are local. Based on this idea we presented the first tunable sub-mm-wave source on CMOS with mW-level output power [38].

The connections in this structure are local in the sense that they are all between adjacent oscillators and there is no long distance interconnect carrying a high frequency signal. The local couplings in this structure are a crucial trait for its further scaling into higher number of cores. However, in the delay-coupled oscillator such a scaling is only possible in a one-dimensional ring. In order to use the two dimensions available on the surface of the chip, we seek to build a source that is scalable in two dimensions, while keeping the advantages of this coupled structure. To develop such a configuration we need to investigate the coupling dynamics of an oscillator in the presence of multiple injecting sources.

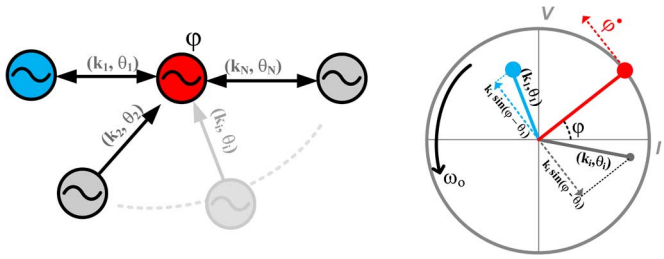

Fig. 2. Phase dynamics of a system of multiple coupled oscillators.

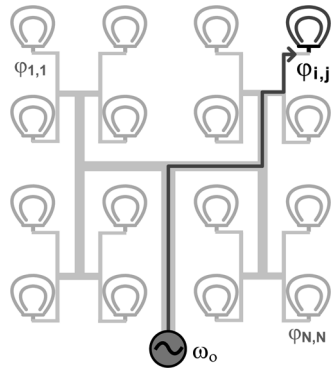

Fig. 3. A conventional phased array structure with global interconnections.

A. A Generalized Form for Adler's Equations

In a more general scheme shown in Fig. 2, an oscillator can on one side couple energy to more than one oscillator and on the other side receive energy from multiple oscillators. To find the dynamics of this generalized scheme we make two assumptions that are also shared by Adler's equations: 1) the coupled energy only affects the phase dynamics and has no significant effect on the amplitude, and 2) the injected energy to an oscillator acts as a vector in the phase space that linearly adds to the phasor of the core oscillator.

Let us consider a core oscillator with a free running frequency of ω_o, which is equal to the time derivative of the oscillator phasor, or $\dot{\varphi} = \omega_o$. In the presence of external injecting sources this equation is perturbed by any extra term that affects the phase derivative. As shown in Fig. 2, only the components of the injecting energy phasor along $\dot{\varphi}$ contribute to the phase dynamics of the core oscillator. As a result, the new phase equation for the core oscillator becomes:

$$\dot{\varphi} = \omega_o + \sum_i k_i \sin(\theta_i - \varphi). \tag{1}$$

This general equation applies to all oscillators in a coupled network regardless of their center frequencies, and locking condition. In the next section we use this general form of Adler's equation to analyze the dynamics of the two-dimensional phased array.

B. A Phased Array Suitable for Terahertz

Because of the coherent combining in a phased array, a terahertz phased array has the potential to overcome the limited available power of any optimally designed single source. In fact, a spatially coherent source is more energy efficient than an equally high power single source. An N element array each with a radiating power of P_o, has an effective isotropically radiated power of $N^2 P_o$, which is N times higher than what is achievable by increasing the power of a single source by a factor of N. This is due to the higher directivity of the phased array configuration. Furthermore, since the number of distributed array elements fitting in a given area increases proportional to $1/\lambda^2$, with the frequency entering the sub-mm-wave region, the higher number of these available coherent sources can substantially compensate for the reduced power of a single source. However, to fully exploit these advantages for terahertz signal generation, we require a scalable physical implementation of the phased array concept.

An ideal phased array consists of a network of radiating elements that are separated by a fixed distance equal to half of the radiation wavelength. All of these elements should radiate simultaneously with equal frequency and a fixed phase shift between adjacent nodes. The conventional implementation of this concept as shown in Fig. 3 is based on a single oscillator that sets the phase of each radiator in the array through a global distribution network typically connected to a set of tunable phase shifters [4]–[9]. This topology is a suitable choice for systems operating at radio and mm-wave frequencies, well below the cut-off frequency of transistors. However, this all-to-one interconnection network poses inherent limitations with respect to scaling, particularly as the operating frequency of the array approaches the terahertz frequency range. The first limitation is due to the long interconnects between the main oscillator and each radiating node. As the dimensions scale, these lines introduce considerable loss as well as mismatch between the different signal paths [43]. Second, for large arrays symmetric routing along different signal paths is challenging. The complexity of the distribution network introduces undesired effects such as coupling between different array nodes as well as error propagation along independent signal routes which becomes increasingly challenging to predict and compensate for. In other words at higher frequencies and in the presence of significant interconnection loss and asymmetry between array nodes, the traditional phased array structure is not scalable which limits its application to a small number of nodes.

III. The Scalable Terahertz Source

To realize a high power terahertz phased array, we introduce a novel architecture that 1) avoids long interconnects and only uses connections that can be readily scaled with dimensions, and 2) is symmetric with respect to all different nodes in the array regardless of their location. Fig. 4 presents the concept of a scalable phased array with these requirements in mind. This array is composed of a network of independently radiating elements that are each locally connected to a terahertz oscillator.

Each oscillator is connected to four other oscillators in the neighboring rows and columns. Similar to the delay-coupled oscillator, the connections between neighboring oscillators are unidirectional. Each oscillator injects energy to two of its immediate neighbors at the same row and column. Meanwhile, this oscillator also receives energy from its other two neighboring oscillators. This network of coupled oscillators is intrinsically scalable since each node only relies on nearest neighbor

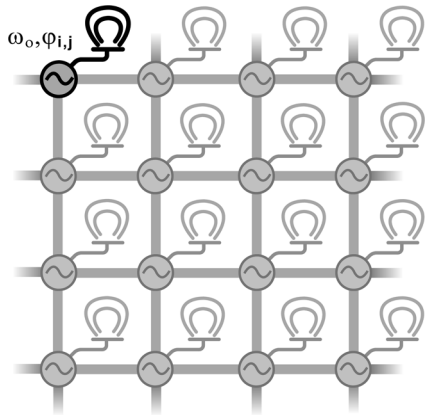

Fig. 4. The proposed phased array structure based on locally coupled radiators.

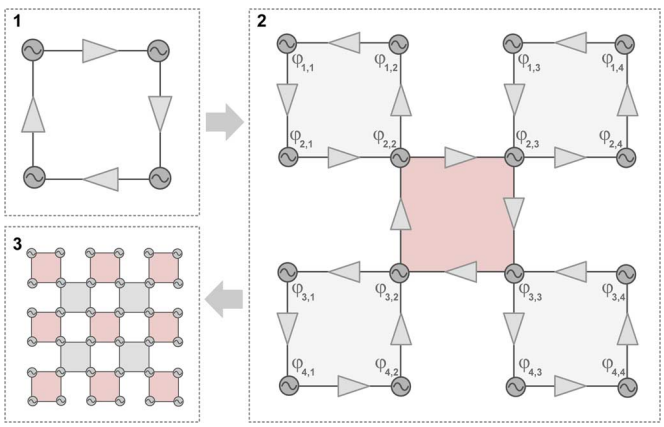

Fig. 5. Construction of the phased array network: (1) 2 × 2, (2) 4 × 4, and (3) 6 × 6.

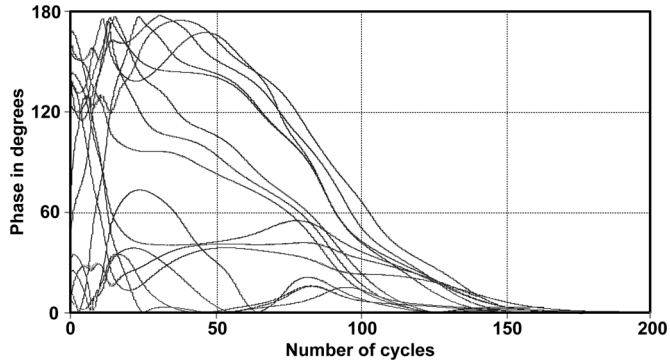

Fig. 6. Phase and frequency synchronization of the 4 × 4 array when each of the 16 oscillators start from a random initial phase.

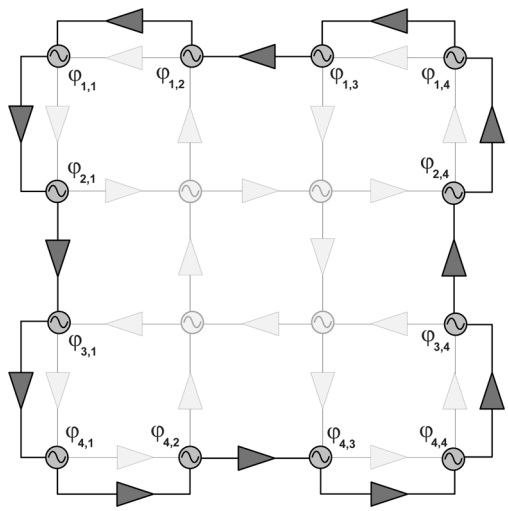

Fig. 7. The 4 × 4 array with auxiliary couplers introduced at the boundaries.

links. Also as we show, the structure can be designed in a way that maintains physically similar coupling dynamics between all oscillators regardless of their location in the network. Unlike global distributions, any mismatch between oscillators and couplers are evenly distributed across the grid. As a result, this distributed coupling is also advantageous in the sense that it does not lead to error propagation throughout different routes.

For this network to act as a phased array all oscillators should first synchronize to a single operating frequency. Furthermore, a mechanism should properly adjust the 2-dimensional phase profile of the lattice in order to steer the beam toward the desired spatial angle. Next, we discuss the process of synchronization and beam steering in this phased array.

A. Core Synchronization

To construct a coupled oscillator array with predictable coupling modes, we begin with a single ring of delay-coupled oscillators. As shown in Fig. 5, we use the ring of four cores as the primary building block. This four-core loop is a suitable choice because it allows a square lattice construct which is a favorable topology for on-chip implementation. Using this building block, we introduce a technique to build a lattice that is scalable and at the same time provides stable coupling modes. To expand the lattice we connect the loops from their vertices. This method permits the construction of patterns with an even number of rows and columns.

A vital feature of the scaling method is that it maintains the basic four-core loops and does not introduce extra loops into the coupled system. For instance in Fig. 5, the four by four array consists of four loops at the four sides. The loops are coupled and synchronized together through a fifth loop at the center. This central loop shares one node with each of the other four. This construction method ensures that the coupling modes behave similar to what is predicted for the delay-coupled loop [44]. Initially and in the absence of coupling, all cores start oscillating at their free running frequency and a random phase. However, as soon as we turn on the couplers and regardless this of initial phase condition, all cores synchronize to the coupling mode that corresponds to equal frequency and equal phase. Numerical simulations confirm that by using this structure, in-phase coupling is possible starting from any initial condition on the oscillators prior to coupling. Fig. 6 demonstrates numerical simulation of frequency and phase synchronization for a network of 16 core oscillators starting with a random initial phase.

B. Symmetric Dynamics

In the configuration shown in Fig. 5.2, the oscillators that are connected in all four sides, receive energy from two neighboring

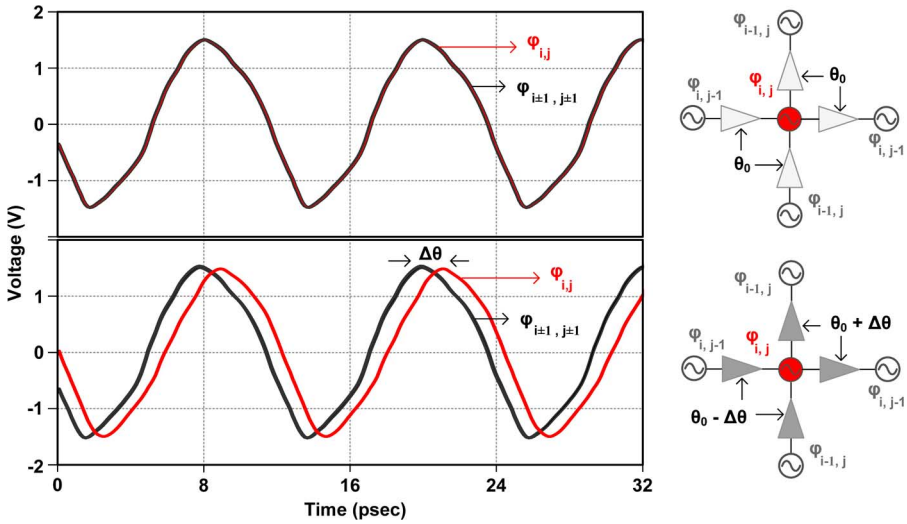

Fig. 8. Simulated waveforms of a core oscillator and its four neighboring elements. Top: equal phase shift applied to all phase shifters. Bottom: A differential phase shift of $\Delta\theta$ applied to modify the phase of the selected core.

cores at their previous or next row and column. After oscillators are synchronized, the phase dynamics of these oscillators can be described by applying (1) for the 2-dimensional array:

$$\frac{d\varphi_{i,j}}{dt} = \omega_o + k^{i,j}_{i\pm1,j}\sin\left(\varphi_{i\pm1,j} + \theta^{i,j}_{i\pm1,j} - \varphi_{i,j}\right) + k^{i,j}_{i,j\pm1}\sin\left(\varphi_{i,j\pm1} + \theta^{i,j}_{i,j\pm1} - \varphi_{i,j}\right) \quad (2)$$

where $\varphi_{i,j}$ is the phase of the oscillator in the ith row and jth column. Furthermore, k^B_A and θ^B_A correspond to the coupling coefficient and phase shift of the coupler that connects node A to node B in the array. This equation is however slightly different for nodes at the edges of the array, where there is only one injecting signal into the oscillator. In such a case, the dynamical equation is a modified version of (2) which includes only one of the injecting terms. Moreover, these oscillators only inject energy to one neighbor that results in a different output loading compared to the central nodes. Thus, the array structure with the present configuration still contains a systematic dynamical mismatch between the elements in the boundaries compared to those at the center.

In order to eliminate this mismatch, we complement these singular nodes with auxiliary couplers at the boundaries of the array. As shown in Fig. 7, these couplers connect in parallel to the main couplers and introduce an equal amount of phase shift and loading. One can easily find that after this modification, the dynamics of all oscillators follow (2), eliminating any location dependency in the coupling dynamics. Now, as a result of this symmetry, in the default case where all the couplers throughout the network are similarly biased, all elements of the array radiate with the same frequency and phase, creating a radiated beam that is perpendicular to the array plane.

C. Beam Forming and Frequency Tuning

The topology in Fig. 7 forms a 2-dimensional grid of radiators where each node can be described by its unique phase. The collection of the individual phases results in a 2-D phase profile consisting of $\varphi_{i,j}$'s. In the case of equal coupling all $\varphi_{i,j}$'s are equal. Nevertheless, it is desirable to generate different phase profiles as it allows manipulating the beam pattern in various ways.

In order to change the phase profile in a particular fashion, we first need a method to independently change the phase of any given oscillator. The dynamics of an oscillator from (2) suggests that changing the phase of an oscillator by a specific amount requires an equal change in the phase of the injected energy into that oscillator from the couplers. In other words one should have a means to change the phase shift, θ, due to the coupling from other neighbors. This can be done by employing tunable phase shifters in the couplers.

At the same time, such a change in θ's and the oscillator phase should not affect the phases of the rest of the nodes in the lattice. Otherwise, this perturbation will propagate and modify the entire phase grid. Since this oscillator also injects energy to two other neighbors, any change in its phase should be compensated by an equally reverse change in the outgoing phase shifters. This means that to increase/decrease the phase shift of an oscillator, one has to increase/decrease the phase shift of incoming couplers and at the same time equally decrease/increase the phase shift of the outgoing coupler. For instance, to change the phase of the (i,j) element of the grid by $\Delta\theta$, the injecting phase shifter $\theta^{i,j}_{i\pm1,j}$ and $\theta^{i,j}_{i,j\pm1}$ should change by $\Delta\theta$ and the outgoing phase shifters $\theta^{i\mp1,j}_{i,j}$ and $\theta^{i,j\mp1}_{i,j}$ should change by $-\Delta\theta$. Such a differential change in the two pairs of couplers will change the phase shift of a single oscillator without modifying the rest of the network. Fig. 8 presents the time-domain behavior of the array with the proposed phase tuning method.

This operation is linear with respect to the oscillator phases and can be independently applied to any node in the network. By superimposing multiple phase operations any desired phase profile can be achieved. It is important to realize that since this differential change in one oscillator does not affect the rest of the lattice, it also follows that it does not alter the locking frequency of the network.

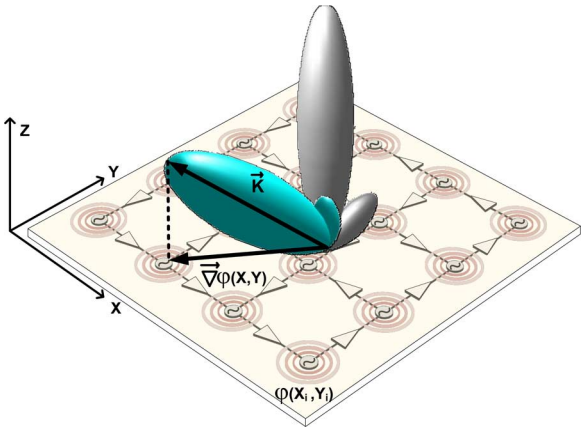

Fig. 9. Beam forming as a result of a 2-D gradient in the phase profile of the oscillators.

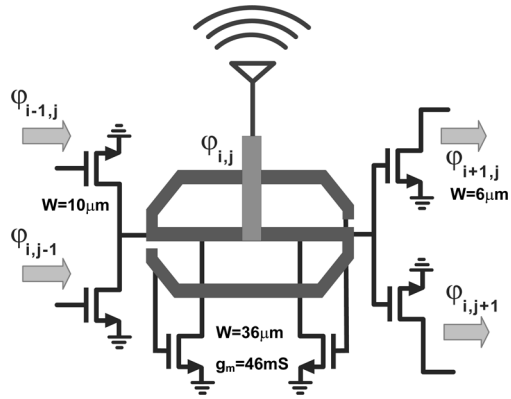

Fig. 10. The core oscillator with the distributed network, the injecting inputs and the outgoing buffers.

In a phased array application we intend to produce the set of $\varphi_{i,j}$'s that maintain the focused beam while steering it along the orthogonal spatial angles. In order to steer the beam into the direction of a particular wave vector K, as shown in Fig. 9, the collection of the phases of the oscillators should create a gradient along this spatial direction.

We can consider steering along the elevation angle for two orthogonal cases: azimuth angles of 0 degrees, and 90 degrees. In Fig. 9, a differential change in the phase of couplers along the X axis results in steering the beam along the first azimuth angle. Similarly, a differential phase change for coupler along the Y axis results in beam steering along the perpendicular azimuth angle. To steer along any other azimuth angle one has to perform a linear superposition of these two orthogonal directions. Any angle can be realized by changing the differential phase shift along the columns and rows. In other words, there is a unique correspondence between all pairs of differential phase shifts across the rows and columns on one side and the 2-dimensional angles on the other side.

The next step is to control the locking frequency of the coupled network. As (2) suggests, by changing all the phase shifters together, the frequency of all oscillators change together while maintaining the phase relation between adjacent cores. This process is similar to the method applied for frequency tuning in the delay-coupled oscillators, where the tuning range depends on the coupling coefficient and the tuning range of the phase shifters.

In summary, changing the phase shifters in a differential manner, results in tuning the beam angle, while changing the common value of the phase shifters tunes the locking frequency. As a result, this phased array structure provides a scalable mechanism to independently control both the beam angle and the locking frequency. Moreover, this control mechanism is evenly applied across the entire grid in a distributed fashion. Such a proposed frequency tuning method also provides a means to modulate the carrier signal should it be used in a transceiver architecture.

IV. Implementation

We implement a fully integrated 4 by 4 terahertz phased array based on the concept proposed in Section III. The terahertz radiator consists of the core oscillators, the coupling network, the phase shifters, and the antennas. Due to the inherent symmetry in the array, each node in the network consists of the same core oscillator and antenna. All neighboring nodes are separated by equal distance and are connected by similar couplers and phase shifters. The next sections describe the details of circuit design and implementation for each of these subsystems.

A. Terahertz Harmonic Oscillator

The core oscillator consists of a pair of NMOS devices that are connected through a distributed resonator shown in Fig. 10. The combination of these two devices and the resonator are adjusted to deliver the maximum generated power at the fourth harmonic frequency to the output load. The size of the core and coupling devices are as shown in Fig. 10. The distributed resonator is a five-port network consisting of a transmission line that connects the gate of one transistor to the drain of another as well as the connection between the drains outputs on one side to the antenna on the other side.

This network performs two separate tasks, first of which is to set the fundamental frequency of the oscillator. The second purpose of the network is to satisfy the power matching criteria between the drain of the transistors and the resistive load of the antenna at the fourth harmonic. To satisfy both of these conditions, the network should provide at least two degrees of freedom. These two can be independently set by tuning the length of the gate and drain connections. Fig. 11 shows the signal paths corresponding to the odd-mode of the network at the fundamental frequency and its even mode at the fourth harmonic. Using the fourth harmonic is a good compromise between lower harmonic numbers with limited fundamental amplitude and higher harmonic numbers with increasingly lower fundamental to harmonic power ratios. In [38], one can find a more detailed argument on the process of selecting the proper harmonic number. The stored energy in this oscillator is distributed across many different elements. Thus, to calculate the quality factor we use its fundamental definition based on the ratio of dissipated energy per cycle over the total stored energy. Using this definition, simulations indicate the quality factor of the oscillator is 15.5 and the distributed resonator is the main contributor to this dissipated energy.

The transmission lines use the top metal layer as the signal layer and the two bottom metal layers as ground. Each core is

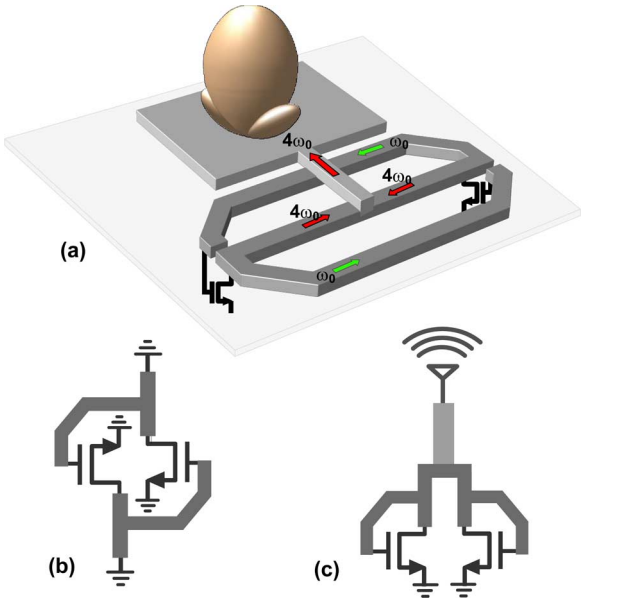

Fig. 11. (a) The core oscillator and radiator indicating the signal paths at the fundamental frequency and the fourth harmonic. Equivalent circuit at the fundamental frequency (b), and at the 4th harmonic (c).

coupled to its four neighboring oscillators. Two couplers on one side of the oscillator inject energy to the core from previous rows and columns. Another two buffers on the other side of the oscillator inject energy from the core to the phase shifters in the next row and columns. These four interfacing devices are considerably smaller in size compared to the core devices. As a result, while isolating the core resonator from the rest of the circuit, they have limited effect on harmonic power generation.

B. Distributed Phase Shifter

The coupling phase shifters connect all adjacent oscillators while providing the necessary phase shift required to adjust the frequency and phase of any given node of the array. In this phased array structure all neighboring cores should be connected through the same coupler circuit. Since each array node is separated from its neighbors by half the wavelength of the radiating frequency, the connection between two adjacent neighbors always contains this fixed distance. Thus, to implement an efficient structure it is appropriate to look for a coupling mechanism that absorbs this distance into the phase shifting process.

The proposed distributed coupler that connects two adjacent cores is shown in Fig. 12. The phase shifter consists of the input buffer from the previous core, the transmission line, and the output energy injecting device. The transmission line is uniformly loaded by six varactors that set the propagating phase shift between the two ends. Fig. 13 shows the simulated quality factor of the varactors and the characteristic impedance of the transmission line as a function of the varactor bias voltage. Here, the control voltage is defined as the difference between the drain and the gate terminals of the varactor. This transmission line is impedance matched with respect to the injecting device at the input and is reflective at the other side. This forms a distributed phase shifter that we tune by changing the value of the varactors. The transmission line provides zero phase shift at the free

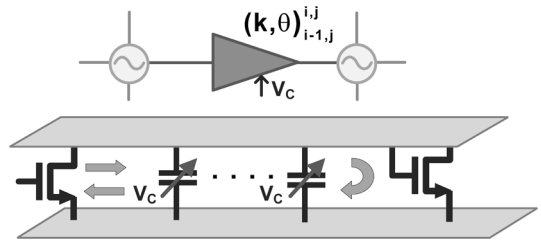

Fig. 12. Distributed phase shifter between adjacent oscillators. The phase shifter operates at the fundamental frequency.

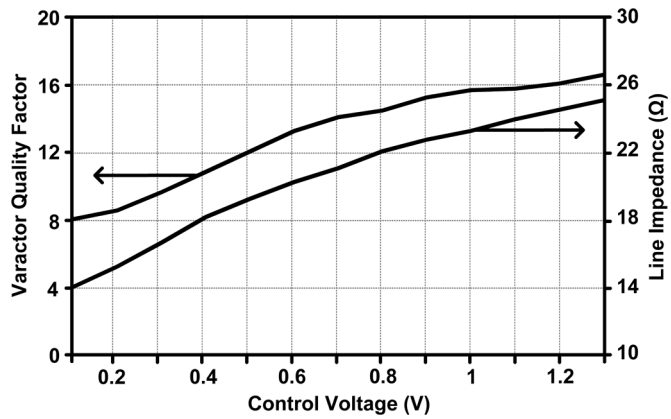

Fig. 13. Simulated quality factor of the varactors and the characteristic impedance of the phase shifter.

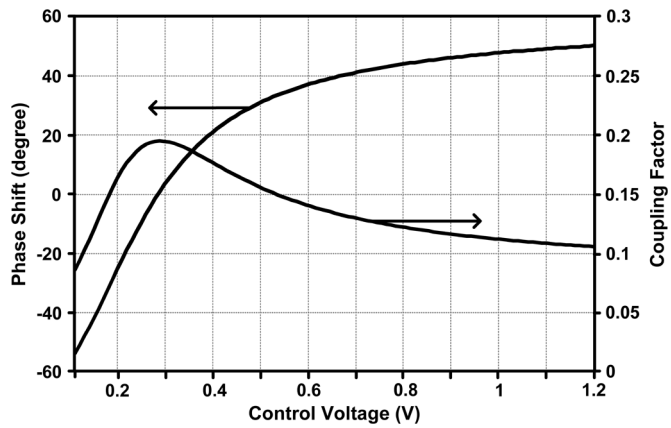

Fig. 14. Simulated phase (θ) and coupling factor (k) of the phase shifter as a function of the applied control voltage.

running frequency of the oscillators resulting in an in-phase coupling for this initial value. At the fundamental frequency, the injected energy is translated through the coupler with zero phase shift in order for the locked frequency to match the center frequency of oscillators. Phase and frequency tuning are realized by tuning the phase shifter around this bias point. Fig. 14 shows the simulated phase shift of the coupler as function of the control voltage.

This coupler simultaneously achieves two important design targets: connecting the two neighboring cores and providing phase control over the coupling. By using this structure, even local connections in this phased array structure are efficiently exploited for design purpose. Furthermore, since the phase shifters avoid inductors as a means of creating resonance, they

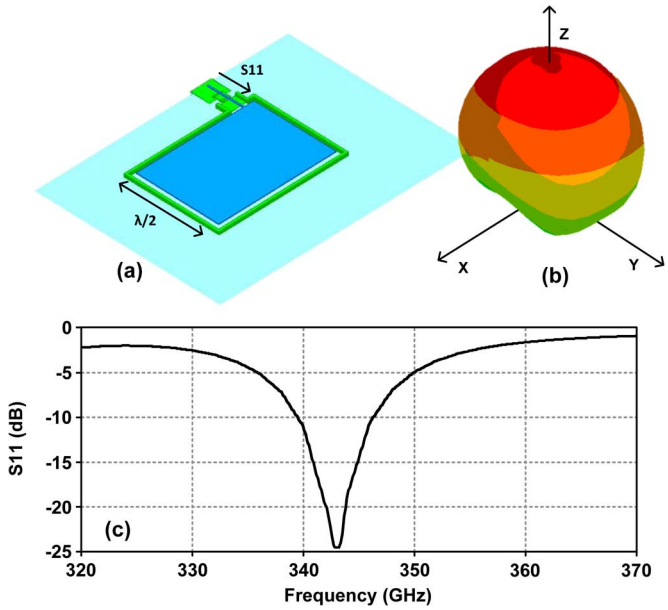

Fig. 15. (a) Structure of the patch antenna. (b) The simulated radiation pattern. (c) The simulated bandwidth.

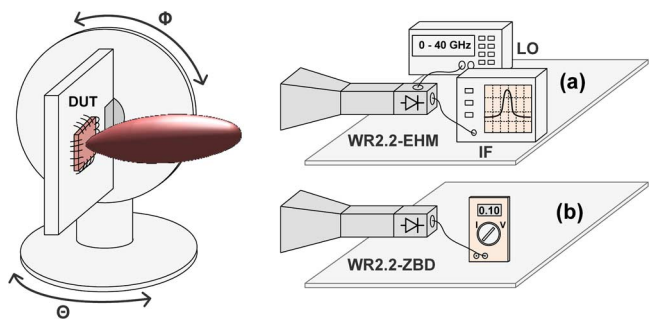

Fig. 16. Measurement setup for (a) phase noise and frequency range of the array, and (b) the radiation pattern and the beam steering. The two rotating plates measure the beam along the two orthogonal angles: Φ and Θ.

lead to a low profile and scalable design. While this implementation includes a single stage coupler, it is possible to increase the tuning range of the phase shifter by cascading multiple stages. This can be useful for applications that requires more phase tuning and/or a larger coupling coefficient.

C. Terahertz Integrated Radiation

The sub-mm dimensions of terahertz wavelengths permits the integration of antenna with the rest of the circuit that can result in a cost-efficient and low-profile phased array. However in order to implement any radiation mechanism on silicon one has to address the adverse effects of substrate coupling. Due to the high refraction index of silicon with respect to air, most of the on-chip radiated energy excites the substrate modes resulting in loss and undesired radiation patterns. With a fixed substrate thickness, substrate coupling increases with frequency. As a result, this phenomena becomes more serious for terahertz frequencies where the radiating wavelengths are comparable with the thickness of bulk silicon substrate. Prior radiation methods have employed silicon lens in order to guide the substrate coupled energy into the desired direction [33], [35], [36]. Using a

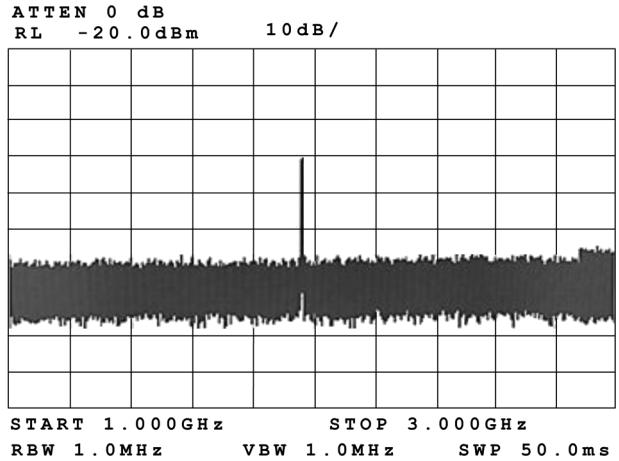

Fig. 17. Measured spectrum of the chip at 338 GHz.

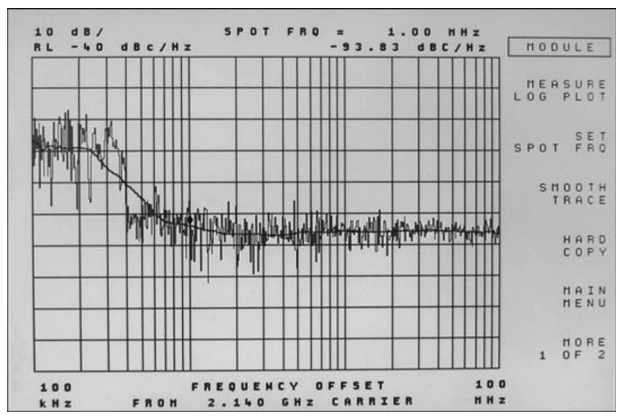

Fig. 18. Measured phase noise radiated from the chip at 338 GHz.

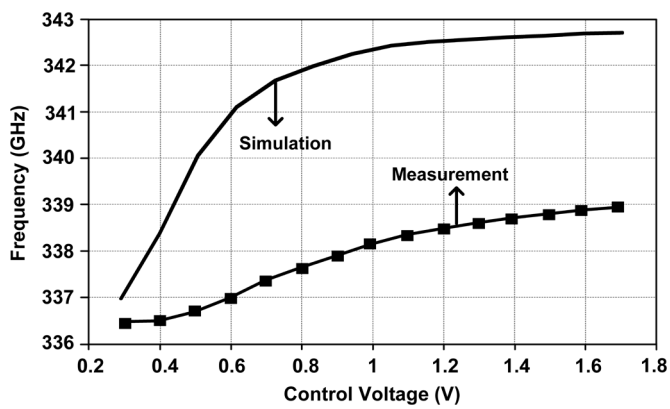

Fig. 19. Simulated and measured frequency tuning range as a function of the phase shifter control voltage.

silicon lens not only increases the cost of the terahertz source, but also prevents any electrical control on the beam angle. Alternatively it is possible to reduce the substrate thickness in order to cancel all coupling modes [34].

Finally, a third method to avoid coupling is to shield the substrate and perform front-side radiation using a patch antenna. A patch antenna has several advantages that become even more prominent as the frequency increases. First, it avoids any substrate coupling which results in a fully integrated radiation

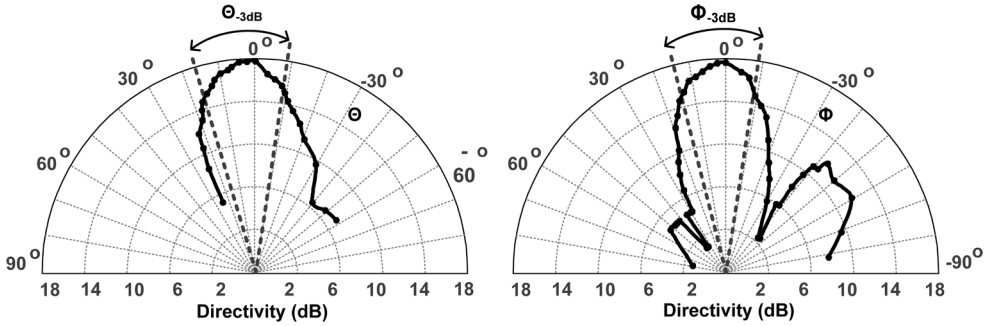

Fig. 20. Measured radiated beam of the array along orthogonal angles at 338 GHz.

mechanism without the need for extra components or post processing. Second, in a phased array structure it also minimizes coupling between adjacent antennas due to its inherent shielding. Finally, the bandwidth of this antenna is a function of the electrical distance between the signal and ground layers which can be adjusted to a desired range. However, this dependence of properties of the patch antenna on its electrical thickness can also become problematic. In a typical CMOS process, around 340 GHz the widest available metal distance results in a patch bandwidth of only 15 GHz which is much smaller than a dipole-based antenna. As a result, to maintain power matching it is essential to take extra care in modeling the center frequency of the antenna and carefully aligning it with the frequency of the source.

Fig. 15 shows the structure of the patch antenna along with its feed from the oscillator output. The length of the antenna is $\lambda/2$ at 340 GHz, while its width is adjusted for the target radiation impedance. Since the patch acts as a leaky resonator that radiates through the electromagnetic field formed around its periphery, shielding the antenna using metal walls does not compromise the radiation pattern [45]. For simulation, we use HFSS to extract the S-parameters of the antenna along with the distributed oscillator network and model it along with the rest of the circuit.

D. Power Supply Distribution

The supply is provided by a quarter wavelength line to the center tap of the resonator. In order to accommodate for the large amount of current distributed across the chip we have created a multilayer plane of supply and ground using four metal layers. This plane propagates across the entire surface except for the areas inside the resonators. The simulated characteristic impedance of the plane is less than 0.1 Ω, which minimizes supply voltage ripples due to high frequency currents.

In our present implementation the supply is provided by wirebonds from the boundaries of the array. As a result, the total current handling of the chip is proportional to the array perimeter while the total current increases proportional to the number of cores, thus proportional to the area. In this configuration, current distribution approach will eventually become a bottleneck in further scaling of thee array. However, using 3D packaging techniques it is possible to provide distributed supply currents across the array and alleviate the limitations of power supply distribution from the chip boundaries.

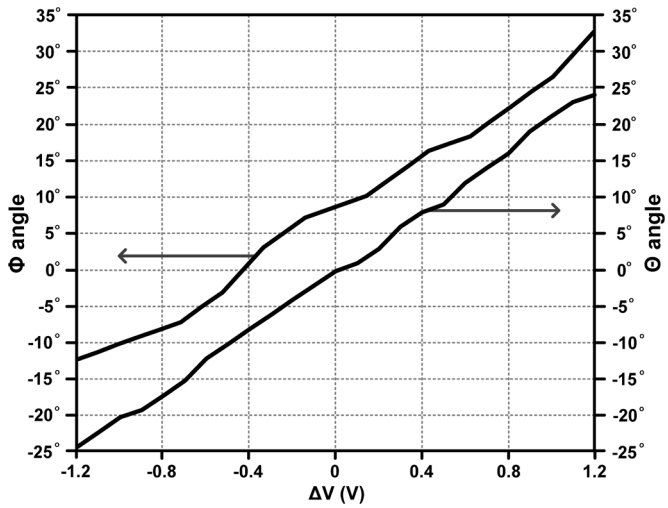

Fig. 21. Measured beam steering across the orthogonal angles as a function of the differential control voltage (ΔV) applied to the phase shifters across rows for Φ, and across columns for Θ.

V. Measurement

The chip prototype is fabricated in a TSMC 65 nm bulk CMOS process. The source contains a tunable array of 16 radiators operating at 340 GHz, which demonstrates the first fully integrated terahertz phased array on CMOS [46]. The DC supply to the core oscillators and the couplers are separated and their values are 1.2 V and 1.1 V, respectively. The measurement setup is shown in Fig. 16. In order to measure the beam pattern, the chip is mounted on a plane that can be rotated along orthogonal angles. For frequency measurement, the receiving horn antenna is connected to a VDI harmonic mixer that down-converts the terahertz signal with the 12th harmonic of the LO frequency.

When oscillator coupling is in effect, the measured radiated frequency of the source is 338 GHz. Fig. 17 shows the measured spectrum and Fig. 18 shows the measured phase noise is -93 dBc/Hz at a 1 MHz offset from the center frequency. To the extent of our knowledge this is lowest measured phase noise compared to any previous radiating electronic source above 100 GHz. This is a result of the coherent combining of multiple sources possible in this phased array, which leads to a phase noise beyond the limits of a single source. The measured phase noise is however an upper limit of the actual phase noise due to the excess noise introduced by the harmonic mixer. As

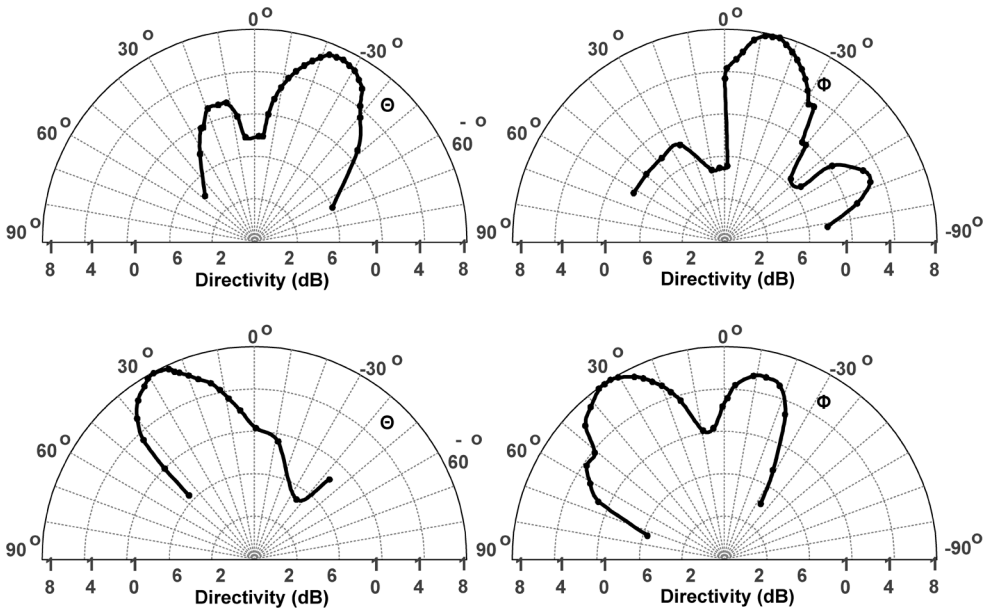

Fig. 22. Measured radiation pattern and beam steering across the two orthogonal angles.

Fig. 18 shows this excess noise dominates the noise floor for frequencies more than 1 MHz away from the center frequency.

By tuning the common value of the coupling phase shifts the center frequency is tuned from 337 GHz to 339 GHz as shown in Fig. 19. Further tuning is possible by changing the supply voltage of the couplers. This would change the g_m of the coupling devices which modulates the coupling coefficient and increases the frequency tuning range. However, a preferred method for increasing the tuning range is to use a multi-stage version of the proposed phase shifter.

The coupling mode of the array can be indirectly verified by the measured output power spectrum. Since the array oscillators and phase shifters are optimized for in-phase coupling, the expected simulated output power is only achievable at this particular coupling mode.

In order to observe the beam pattern and beam steering, we use a VDI zero bias detector. Using this detector we measure the relative power at different angles between the chip and the receiving horn antenna. As shown in Fig. 20, the radiated beam at 338 GHz has -3 dB beam widths of 24 degrees and 27 degrees in the two orthogonal angles. Integrating this beam pattern in spherical coordinates results in an a antenna directivity of 18 dB [47]. Subtracting the 12 dB due to the array gain, yields a measured antenna directivity of 6 dB for the patch antenna which is in agreement with simulations. Next, by differential tuning of the phase shifters we measure the change in the direction of the beam. A differential change in the array columns steers the beam along the Θ angle and a differential change in the array rows steers the beam along the Φ angle. The measured beam angle is shown as a function of the control voltage in Fig. 21. The beam steering is 50 degrees in Φ and 45 degrees in Θ. Most likely, the bias present in the measured Φ angle is due to a tilt in the measurement setup. A wider tuning range is also possible by increasing the tuning range of the phase shifters using the method described in Section III. Fig. 22 shows the radiation pattern when the antenna is steered in four different angles.

A wide-band calorimeter connected to the horn antenna measures the radiated power from the chip. This method is wideband by nature and as a result detects any thermal radiation from the chip within the detector bandwidth. In order to subtract any spurious detected energy we perform the following procedure: First the core oscillators are turned on in the absence of coupling. This creates incoherent radiation which is undetectable compared to the black body radiation received from the chip. Next, the couplings are turned on resulting in coherent radiation. Since the chip temperature does not change due to coupling, the measured increase in the detected power is entirely due to the terahertz radiated signal.

For a matched impedance, the simulated power at the second harmonic is 10 dB higher than the fourth harmonic power. However, the narrowband nature of the patch antenna largely suppresses this harmonic. Furthermore, the high-pass cut-off frequency of the antenna and rectangular waveguides on the receive side are much higher than the second harmonic frequency. As a result, the measured signal power is entirely due to the fourth harmonic of the oscillators around 340 GHz. Fig. 23 shows the measured power received by the detector as a function of its distance to the chip which agrees with the Friis equation for electromagnetic radiation [48].

The equivalent isotropically radiated power (EIRP) is derived from this measurement by de-embedding the loss due to the distance between the chip and the receiving antenna. The total power radiated from the chip is subsequently derived by subtracting the measured antenna directivity of the chip from the EIRP. For a fixed distance, Fig. 24 shows the measured EIRP and total radiated power from the chip for different control voltages. The measured peak EIRP of the chip is 51 mW at 338 GHz and the peak total radiated power is 0.8 mW. Fig. 25 shows the chip micro-photo indicating its main building blocks. Table I compares the performance of this chip with prior art. This chip demonstrates the highest radiated power, the highest EIRP, and

TABLE I
COMPARISON WITH PRIOR ART

Reference	[34]	[35]	[36]	[37]	This Work
Frequency (GHz)	280	288	260	380	338
Total Power (dBm)	-7.2*	-4.1**	0.5**	-17.3	-0.9
Peak EIRP (dBm)	9.4	N/A	15.7	-11	17.1
Freq. Tuning (%)	3.2	Non-tuning	1.4	0.9	2.1***
Phase Noise (@ 1MHz offset)	N/A	-87	-78.3	N/A	-93
Beam Steering	80/80	Fixed pattern	Fixed pattern	Fixed pattern	45/50
DC Power (W)	0.81	0.28	0.8	0.38	1.54
Technology	45 nm SOI CMOS	65 nm bulk CMOS	65 nm bulk CMOS	130 nm SiGe BiCMOS	65 nm bulk CMOS
Area (mm^2)	7.2	0.32	2.25	4.1	3.9

* Substrate-thinning used for front-side radiation
** A Hemispheric lens is used for back-side radiation
*** Includes 10% variation in the phase shifter supply voltage

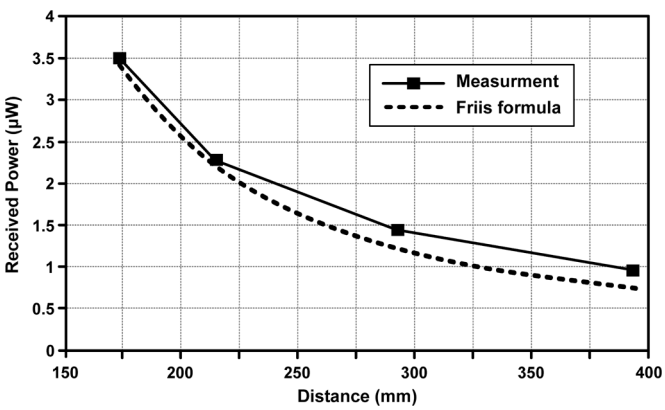

Fig. 23. Measured received power as a function of the receiver distance from the chip.

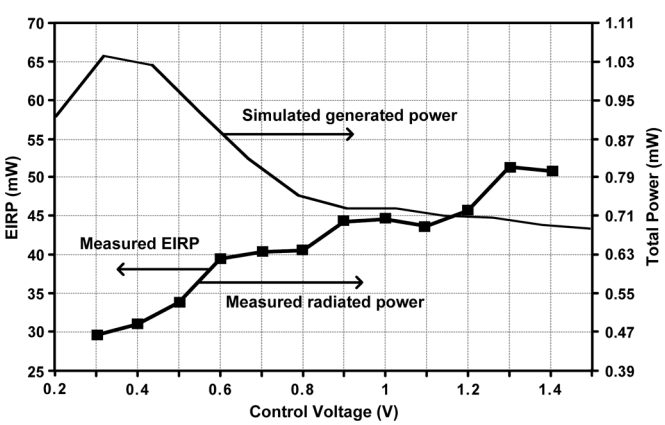

Fig. 24. Measured EIRP and total radiated power from the chip and the simulated total generated power.

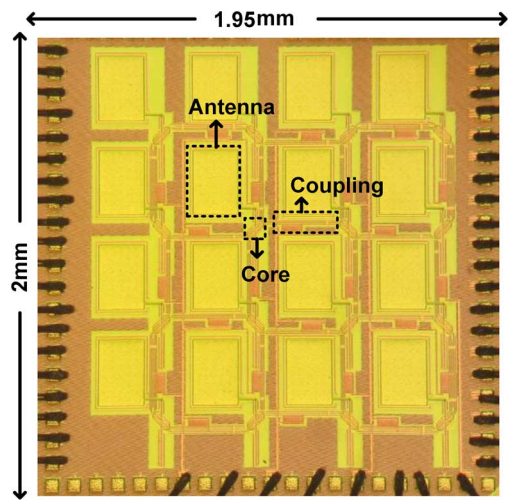

Fig. 25. Chip micro photo.

the lowest phase noise in a terahertz silicon source without using any extra components or post processing.

VI. CONCLUSION

The extension of the operating frequency of silicon integrated systems into terahertz frequencies faces fundamental obstacles due to the limits of individual devices and circuits. To overcome these limitations, in this work we propose a collective approach toward terahertz signal generation that employs large number of devices in a fully scalable fashion. Using this method we present a scalable terahertz phased array that demonstrates a radiated power level and spectral purity that is beyond what is achievable by conventional sources and

phased arrays. This demonstrated technique paves the way for high power generation at terahertz frequencies using CMOS technology. Furthermore, the presented technique can be employed by compound semiconductor technologies to achieve even higher power levels at higher operating frequencies.

REFERENCES

[1] N. Saito *et al.*, "A fully integrated 60-GHz CMOS transceiver chipset based on WiGig/IEEE 802.11ad with built-in self calibration for mobile usage," *IEEE J. Solid-State Circuits*, vol. 48, no. 12, pp. 3146–3159, Dec. 2013.

[2] S. Shahramian, Y. Baeyens, and Y.-K. Chen, "A 70–100 GHz direct-conversion transmitter and receiver phased array chipset demonstrating 10 Gb/s wireless link," *IEEE J. Solid-State Circuits*, vol. 48, no. 5, pp. 1113–1125, May 2013.

[3] N. Pohl, T. Klein, K. Aufinger, and H. Rein, "A low-power wideband transmitter front-end chip for 80 GHz FMCW radar systems with integrated 23 GHz downconverter VCO," *IEEE J. Solid-State Circuits*, vol. 47, no. 9, pp. 1974–1980, Sep. 2012.

[4] J. Chen *et al.*, "A digitally modulated mm-Wave cartesian beamforming transmitter with quadrature spatial combining," in *IEEE ISSCC Dig. Tech. Papers*, 2013, pp. 232–233.

[5] E. Cohen, M. Ruberto, M. Cohen, O. Degani, S. Ravid, and D. Ritter, "A CMOS bidirectional 32-element phased-array transceiver at 60 GHz with LTCC antenna," in *IEEE Radio Frequency Integrated Circuits Symp. Dig.*, 2012, pp. 439–442.

[6] L. Kong, D. Seo, and E. Alon, "A 50 mW-TX 65 mW-RX 60 GHz 4-element phased-array transceiver with integrated antennas in 65 nm CMOS," in *IEEE ISSCC Dig. Tech. Papers*, 2013, pp. 234–236.

[7] A. Moroni, R. Genesi, and D. Manstretta, "Analysis and design of a 54 GHz distributed 'Hybrid' wave oscillator array with quadrature outputs," *IEEE J. Solid-State Circuits*, vol. 49, no. 5, pp. 1158–1172, May 2014.

[8] W. Shin, B. Ku, O. Inac, Y.-C. Ou, and G. M. Rebeiz, "A 108–114 GHz 4×4 wafer-scale phased array transmitter with high-efficiency on-chip antennas," *IEEE J. Solid-State Circuits*, vol. 48, no. 9, pp. 2041–2055, Sep. 2013.

[9] A. Valdes-Garcia *et al.*, "A fully integrated 16-element phased-array transmitter in SiGe BiCMOS for 60-GHz communications," *IEEE J. Solid-State Circuits*, vol. 45, no. 12, pp. 2757–2773, Dec. 2010.

[10] K. Kawasaki *et al.*, "A millimeter-wave intra-connect solution," *IEEE J. Solid-State Circuits*, vol. 45, no. 12, pp. 2655–2666, Dec. 2010.

[11] B. P. Ginsburg, S. M. Ramaswamy, V. Rentala, E. Seok, S. Sankaran, and B. Haroun, "A 160 GHz pulsed radar transceiver in 65 nm CMOS," *IEEE J. Solid-State Circuits*, vol. 49, no. 4, pp. 984–995, Apr. 2014.

[12] V. Giannini *et al.*, "A 79 GHz phase-modulated 4 GHz-BW CW radar TX in 28 nm CMOS," in *IEEE ISSCC Dig. Tech. Papers*, 2014, pp. 250–251.

[13] J. Lee, Y.-A. Li, M.-H. Hung, and S.-J. Huang, "A fully-integrated 77-GHz FMCW radar transceiver in 65-nm CMOS technology," *IEEE J. Solid-State Circuits*, vol. 45, no. 12, pp. 2746–2756, Dec. 2010.

[14] A. Arbabian, S. Callender, S. Kang, M. Rangwala, and A. M. Niknejad, "A 94 GHz mm-wave-to-baseband pulsed-radar transceiver with applications in imaging and gesture recognition," *IEEE J. Solid-State Circuits*, vol. 48, no. 4, pp. 1055–1071, Apr. 2013.

[15] P. Chen, P. Peng, C. Kao, Y. Chen, and J. Lee, "A 94 GHz 3D-image radar engine with 4TX/4RX beamforming scan technique in 65 nm CMOS," in *IEEE ISSCC Dig. Tech. Papers*, 2013, pp. 146–148.

[16] F. C. Ii, L. Gilreath, S. Pan, Z. Wang, F. Capolino, and P. Heydari, "Design and analysis of a W-band 9-element imaging array receiver using spatial-overlapping super-pixels in silicon," *IEEE J. Solid-State Circuits*, vol. 49, no. 6, pp. 1317–1332, Jun. 2014.

[17] Y. Mao, K. Schmalz, J. Borngräber, J. C. Scheytt, and C. Meliani, "245 GHz subharmonic receivers in SiGe," in *IEEE Radio Frequency Integrated Circuits Symp. (RFIC) Dig.*, 2013, pp. 101–104.

[18] E. Öjefors, B. Heinemann, and U. R. Pfeiffer, "A 220 GHz subharmonic receiver front end in a SiGe HBT technology," in *IEEE Radio Frequency Integrated Circuits Symp. Dig.*, 2011, pp. 11–14.

[19] K. Schmalz, J. Borngräber, B. Heinemann, H. Rücker, and J. C. Scheytt, "A 245 GHz transmitter in SiGe technology," in *IEEE Radio Frequency Integrated Circuits Symp. Dig.*, 2012, pp. 195–198.

[20] C. Bredendiek, N. Pohl, T. Jaeschke, K. Aufinger, and A. Bilgic, "A 240 GHz single-chip radar transceiver in a SiGe bipolar technology with on-chip antennas and ultra-wide tuning range," in *IEEE Radio Frequency Integrated Circuits Symp. (RFIC) Dig.*, 2013, pp. 309–312.

[21] Z. Wang, P. Chiang, P. Nazari, C.-C. Wang, Z. Chen, and P. Heydari, "A CMOS 210-GHz fundamental transceiver with OOK modulation," *IEEE J. Solid-State Circuits*, vol. 49, no. 3, pp. 564–580, Mar. 2014.

[22] L. A. Samoska, "An overview of solid-state integrated circuit amplifiers in the submillimeter-wave and THz regime," *IEEE Trans. Terahertz Sci. Technol.*, vol. 1, no. 1, pp. 9–24, 2011.

[23] M. Seo *et al.*, "InP HBT IC technology for terahertz frequencies: Fundamental oscillators up to 0.57 THz," *IEEE J. Solid-State Circuits*, vol. 46, no. 10, pp. 2203–2214, Oct. 2011.

[24] S. P. Voinigescu *et al.*, "A study of SiGe HBT signal sources in the 220–330-GHz range," *IEEE J. Solid-State Circuits*, vol. 48, no. 9, pp. 2011–2021, Sep. 2013.

[25] A. Tessmann, "220-GHz metamorphic HEMT amplifier MMICs for high-resolution imaging applications," *IEEE J. Solid-State Circuits*, vol. 40, no. 10, pp. 2070–2076, Oct. 2005.

[26] R. Han *et al.*, "Active terahertz imaging using Schottky diodes in CMOS: Array and 860-GHz pixel," *IEEE J. Solid-State Circuits*, vol. 48, no. 10, pp. 2296–2308, Oct. 2013.

[27] R. Al Hadi *et al.*, "A 1 k-pixel video camera for 0.7–1.1 terahertz imaging applications in 65-nm CMOS," *IEEE J. Solid-State Circuits*, vol. 47, no. 12, pp. 2999–3012, Dec. 2012.

[28] M. Uzunkol, G. Ozan, D. F. Golcuk, and G. M. Rebeiz, "A 0.32 THz SiGe 4×4 imaging array using high-efficiency on-chip antennas," *IEEE J. Solid-State Circuits*, vol. 48, no. 9, pp. 2056–2066, Sep. 2013.

[29] L. Gilreath, V. Jain, and P. Heydari, "Design and analysis of a W-band SiGe direct-detection-based passive imaging receiver," *IEEE J. Solid-State Circuits*, vol. 46, no. 10, pp. 2240–2252, Oct. 2011.

[30] O. Momeni, "A 260 GHz amplifier with 9.2 dB gain and -3.9 dBm saturated power in 65 nm CMOS," in *IEEE ISSCC Dig. Tech. Papers*, 2013, pp. 140–142.

[31] O. Momeni and E. Afshari, "High power terahertz and millimeter-wave oscillator design: A systematic approach," *IEEE J. Solid-State Circuits*, vol. 46, no. 3, pp. 583–597, Mar. 2011.

[32] A. Arbabian and A. M. Niknejad, "A three-stage cascaded distributed amplifier with GBW exceeding 1.5 THz," in *IEEE Radio Frequency Integrated Circuits Symp. Dig.*, 2012, no. 1, pp. 211–214.

[33] U. R. Pfeiffer *et al.*, "A 0.53 THz reconfigurable source array with up to 1 mW radiated power for terahertz imaging applications in 0.13 μm SiGe BiCMOS," in *IEEE ISSCC Dig. Tech. Papers*, 2014, pp. 256–258.

[34] K. Sengupta and A. Hajimiri, "A 0.28 THz power-generation and beam-steering array in CMOS based on distributed active," *IEEE J. Solid-State Circuits*, vol. 47, no. 12, pp. 3013–3031, Dec. 2012.

[35] J. Grzyb, Y. Zhao, and U. R. Pfeiffer, "A 288-GHz lens-integrated balanced triple-push source in a 65-nm CMOS technology," *IEEE J. Solid-State Circuits*, vol. 48, no. 7, pp. 1751–1761, Jul. 2013.

[36] R. Han and E. Afshari, "A CMOS high-power broadband 260-GHz radiator array for spectroscopy," *IEEE J. Solid-State Circuits*, vol. 48, no. 12, pp. 3090–3104, Dec. 2013.

[37] J. Park, S. Kang, and A. M. Niknejad, "A 0.38 THz fully integrated transceiver utilizing a quadrature push-push harmonic circuitry in SiGe BiCMOS," *IEEE J. Solid-State Circuits*, vol. 47, no. 10, pp. 2344–2354, Oct. 2012.

[38] Y. M. Tousi, O. Momeni, and E. Afshari, "A novel CMOS high-power terahertz VCO based on coupled oscillators: Theory and implementation," *IEEE J. Solid-State Circuits*, vol. 47, no. 12, pp. 3032–3042, Dec. 2012.

[39] P.-Y. Chiang, Z. Wang, O. Momeni, and P. Heydari, "A 300 GHz frequency synthesizer with 7.9% locking range in 90 nm SiGe BiCMOS," in *IEEE ISSCC Dig. Tech. Papers*, 2014, pp. 260–261.

[40] M. Adnan and E. Afshari, "A 247-to-263.5 GHz VCO with 2.6 mW peak output power and 1.14% DC-to-RF efficiency in 65 nm bulk CMOS," in *IEEE ISSCC Dig. Tech. Papers*, 2014, pp. 262–263.

[41] "Radio frequency and analog/mixed-signal technologies," International Technology Roadmap for Semiconductors, ITRS, 2013.

[42] R. Adler, "A study of locking phenomena in oscillators," *Proc. IRE*, vol. 34, no. 6, pp. 351–357, 1946.

[43] J. F. Buckwalter, A. Babakhani, S. Member, A. Komijani, and A. Hajimiri, "An integrated subharmonic coupled-oscillator scheme for a 60-GHz phased-array transmitter," , vol. 54, no. 12, pp. 4271–4280, 2006.

[44] Y. M. Tousi, V. Pourahmad, and E. Afshari, "Delay coupled oscillators for frequency tuning of solid-state terahertz sources," *Phys. Rev. Lett.*, vol. 108, no. 23, p. 234101, Jun. 2012.

[45] C. A. Balanis, "Antenna theory: A review," *Proc. IEEE*, vol. 80, no. 1, pp. 7–23, 1992.
[46] Y. M. Tousi and E. Afshari, "A scalable THz 2D phased array with +17 dBm of EIRP at 338 GHz in 65 nm bulk CMOS," in *IEEE ISSCC Dig. Tech. Papers*, 2014, pp. 258–260.
[47] R. Stegen, "The gain-beamwidth product of an antenna," *IEEE Trans. Antennas Propagat.*, vol. TAP-12, no. 4, pp. 505–506, 1964.
[48] H. Friis, "A note on a simple transmission formula," *Proc. IRE*, vol. 34, no. 5, pp. 254–256, 1946.

Yahya Tousi (S'07–M'11) received the B.S. degree in 2004 and the M.S. degree in 2006, both in electrical engineering from Sharif University of Technology, Tehran, Iran. In 2012 he received the Ph.D. degree from the Department of Electrical and Computer Engineering at Cornell University, Ithaca, NY, USA.

Since 2014, he has been with the IBM T. J. Watson Research Center, Yorktown Heights, NY, USA, with a focus on advanced integrated circuits and systems. Prior to that, from 2012 to 2014 he was an RFIC scientist at SiTune Corporation, San Jose, CA, USA. His current research interests are in novel high-speed integrated circuits and systems for communication, biomedical, and signal processing applications.

Dr. Tousi is the recipient of the 2009 Cornell Jacob Fellowship, the 2011 IEEE Microwave Theory and Techniques Society Graduate Fellowship, and the 2011–2012 IEEE Solid-State Circuits Society Pre-Doctoral Achievement Award. He is also the winner of the Graduate Research Competition at IMS 2011.

Ehsan Afshari (S'98–M'07–SM'11) was born in 1979. He received the B.Sc. degree in electronics engineering from Sharif University of Technology, Tehran, Iran, and the M.S. and Ph.D. degrees in electrical engineering from the California Institute of Technology, Pasadena, CA, USA, in 2003 and 2006, respectively.

In August 2006, he joined the faculty of Electrical and Computer Engineering at Cornell University, Ithaca, NY, USA. His research interests are mm-wave and terahertz electronics and low-noise integrated circuits for applications in communication systems, sensing, and biomedical devices.

Prof. Afshari serves as the chair of the IEEE Ithaca section, as the chair of Cornell Highly Integrated Physical Systems (CHIPS), as a member of International Technical Committee of the IEEE Solid-State Circuits Conference (ISSCC), as a member of the Analog Signal Processing Technical Committee of the IEEE Circuits and Systems Society, as a member of the Technical Program Committee of the IEEE Custom Integrated Circuits Conference (CICC), and as a member of the Technical Program Committee of the IEEE International Conference on Ultra-Wideband (ICUWB). He was awarded the National Science Foundation CAREER Award in 2010, Cornell College of Engineering Michael Tien Excellence in Teaching Award in 2010, the Defense Advanced Research Projects Agency (DARPA) Young Faculty Award in 2008, and Iran's Best Engineering Student Award by the President of Iran in 2001. He is also the recipient of the Best Paper Award in the IEEE Custom Integrated Circuits Conference (CICC), September 2003, the First Place at the Stanford-Berkeley-Caltech Inventors Challenge, March 2005, the Best Undergraduate Paper Award in Iranian Conference on Electrical Engineering, 1999, the recipient of the Silver Medal in the Physics Olympiad in 1997, and the recipient of the Award of Excellence in Engineering Education from Association of Professors and Scholars of Iranian Heritage (APSIH), May 2004.